Quantification of the influence of drugs on zebrafish larvae swimming kinematics and energetics

Zhenkai Zhao [1], **Gen Li** [2], **Qing Xiao** [Corresp., 3], **Huirong Jiang** [4], **Gabriel Mbuta Tchivelekete** [5], **Xinhua Shu** [5], **Hao Liu** [6]

[1] Department of Naval Architecture, Ocean, and Marine Engineering, University of Strathclyde, Glasgow, United Kingdom

[2] Department of Mathematical Science and Advanced Technology, Japan Agency for Marine-Earth Science and Technology (JAMSTEC), Yokohama-city, Japan

[3] Department of Naval Architecture, Ocean, and Marine Engineering, University of Strathclyde, Glasgow, United Kingom

[4] Strathclyde Institute of Pharmacy and Biomedical Sciences, University of Strathclyde, Glasgow, United Kingdom

[5] Department of Biological and Biomedical Sciences, Glasgow Caledonian University, Glasgow, United Kingdom

[6] Graduate School of Engineering, Chiba University, Chiba, Japan

Corresponding Author: Qing Xiao
Email address: qing.xiao@strath.ac.uk

The use of zebrafish larvae has aroused wide interest in the medical field for its potential role in the development of new therapies. The larvae grow extremely quickly and the embryos are nearly transparent which allows easy examination of its internal structures using fluorescent imaging techniques. Medical treatment of zebrafish larvae can directly influence its swimming behaviours. These behaviour changes are related to functional changes of central nervous system (CNS) and transformations of the zebrafish body such as muscle mechanical power and force variation, which cannot be measured directly by pure experiment observation. To quantify the influence of drugs on zebrafish larvae swimming behaviours and energetics, we have developed a novel methodology to exploit intravital changes based on observed zebrafish locomotion. Specifically, by using an in-house MATLAB code to process the recorded live zebrafish swimming video, the kinematic locomotion equation of a 3D zebrafish larvae was obtained, and a customised Computational Fluid Dynamics (CFD) tool was used to solve the fluid flow around the fish model which was geometrically the same as experimentally tested zebrafish. The developed methodology was firstly verified against experiment, and further applied to quantify the fish internal body force, torque and power consumption associated with a group of normal zebrafish larvae versus those immersed in acetic acid and two neuroactive drugs. As indicated by our results, zebrafish larvae immersed in 0.01% acetic acid display approximately 30% higher hydrodynamic power and 10% higher cost of transport than control group. Besides, 500 uM diphenylhydantoin (DPH) significantly decreases the locomotion activity for approximately 50% lower hydrodynamic power, whereas 100 mg/L yohimbine has not caused any significant influences on 5 dpf zebrafish

larvae locomotion. The approach has potential to evaluate the influence of drugs on the aquatic animal's behaviour changes and thus support the development of new analgesic and neuroactive drugs.

1 Quantification of the influence of drugs on zebrafish larvae swimming kinematics and energetics

3 Zhenkai Zhao[1], Gen Li[2], Qing Xiao[1, *], Huirong Jiang[3], Gabriel Mbuta Tchivelekete[4], Xinhua

4 Shu[4] and Hao Liu[5]

5 [1] Department of Naval Architecture, Ocean, and Marine Engineering, University of Strathclyde,

6 Glasgow, United Kingdom

7 Email: z.zhao@strath.ac.uk

8 [2]Department of Mathematical Science and Advanced Technology, Japan Agency for Marine-

9 Earth Science and Technology (JAMSTEC), Yokohama-city, Japan

10 Email: ligen@jamstec.go.jp

11 [3]Strathclyde Institute of Pharmacy and Biomedical Sciences, University of Strathclyde, Glasgow,

12 United Kingdom

13 Email: Huirong.jiang@strath.ac.uk

14 [4] Department of Biological and Biomedical Sciences, Glasgow Caledonian University, Glasgow,

15 United Kingdom

16 Xinhua.Shu@gcu.ac.uk

17 [5] Graduate School of Engineering, Chiba University, Chiba, Japan

18 Email: hliu@faculty.chiba-u.jp

19   *Author for correspondence (qing.xiao@strath.ac.uk)

34   **Abstract**

35   The use of zebrafish larvae has aroused wide interest in the medical field for its potential role in

36   the development of new therapies. The larvae grow extremely quickly and the embryos are

37   nearly transparent which allows easy examination of its internal structures using fluorescent

38   imaging techniques. Medical treatment of zebrafish larvae can directly influence its swimming

39   behaviours. These behaviour changes are related to functional changes of central nervous system

40   (CNS) and transformations of the zebrafish body such as muscle mechanical power and force

41   variation, which cannot be measured directly by pure experiment observation. To quantify the

42   influence of drugs on zebrafish larvae swimming behaviours and energetics, we have developed

43   a novel methodology to exploit intravital changes based on observed zebrafish locomotion.

44   Specifically, by using an in-house MATLAB code to process the recorded live zebrafish

45   swimming video, the kinematic locomotion equation of a 3D zebrafish larvae was obtained, and

46   a customised Computational Fluid Dynamics (CFD) tool was used to solve the fluid flow around

47   the fish model which was geometrically the same as experimentally tested zebrafish. The

48   developed methodology was firstly verified against experiment, and further applied to quantify

49   the fish internal body force, torque and power consumption associated with a group of normal

50   zebrafish larvae versus those immersed in acetic acid and two neuroactive drugs. As indicated by

51   our results, zebrafish larvae immersed in 0.01% acetic acid display approximately 30% higher

52   hydrodynamic power and 10% higher cost of transport than control group. Besides, $500 \mu M$

53   diphenylhydantoin (DPH) significantly decreases the locomotion activity for approximately 50%

54   lower hydrodynamic power, whereas 100 mg/L yohimbine has not caused any significant

55   influences on 5 dpf zebrafish larvae locomotion. The approach has potential to evaluate the

56   influence of drugs on the aquatic animal's behaviour changes and thus support the development

57   of new analgesic and neuroactive drugs.

58

59   **1. Introduction**

60   In the past decade, the zebrafish has been widely used in medical, biological and genetic

61   research. In its embryonic and larval stage, the zebrafish body is nearly transparent, which

62 conveniently allows the observation of fish organs development. Its quick reproduction speed

63 and cheaper cost, compared to other fish species and mouse, give it a unique and important role

64 in scientific research to resolve a wide range of issues. Among those issues, nociception and

65 nervous system functions are significant and extensively studied. Nociception is a sensory

66 mechanism used to perceive tissue damage (Gregory et al., 2013). Noxious stimuli detected by

67 nociceptors responding to thermal (Malafoglia et al., 2014), electrical (Roques, Abbink, Geurds,

68 van de Vis, & Flik, 2010) and chemical (Mettam, McCrohan, & Sneddon, 2012) stimulation can

69 cause acute or chronic pain. zebrafish share similar nociceptive responses to those of human

70 adults (Malafoglia, Bryant, Raffaeli, Giordano, & Bellipanni, 2013), it is prudent to use the

71 zebrafish larva model to test new analgesic drugs for pain relief. Morphine has been tested on

72 adult zebrafish as an analgesic drug to alleviate the pain caused by acetic acid and shown to have

73 positive effects for pain alleviation. This was achieved via experimental observation and data

74 analysis on fish swimming behaviour changes, such as distance travelled and averaged

75 swimming velocity(Correia, Cunha, Scholze, & Stevens, 2011; Taylor et al., 2017). Furthermore,

76 more noxious stimuli and drugs have been tested using larvae zebrafish, showing that larvae

77 respond to a noxious challenge in a similar way as adult zebrafish, and the nociceptive response

78 is induced by acetic acid(Lopez-Luna, Al-Jubouri, Al-Nuaimy, & Sneddon, 2017a), which makes

79 it possible to replace protected adult zebrafish with larvae for nociception research.

80

81 Administration of neuroactive drugs is an effective method to test animal's nervous system

82 functions (Irons, MacPhail, Hunter, & Padilla, 2010).As neuroactive drugs acting on different

83 neural pathways could cause different behavioural phenotypes, it is possible to study how the

84 nervous system affects locomotion behaviours by applying different neuroactive drugs (F. Li et

85 al., 2018). Zebrafish shares similar structure and functions of nervous system compared to

86 mammalian (Anderson & Ingham, 2003; Xi et al., 2010), and has been validated to study neural

87 effects on behavioural manifestation (Sison, Cawker, Buske, & Gerlai, 2006). A commonly used

88 drug ethanol was studied to determine the acute and chronic effects on zebrafish behaviours and

89 resulted in different types of behaviour alterations such as time spent active, leaping frequency

90 and distance from stimulus (Dlugos & Rabin, 2003; R. Gerlai, Lahav, Guo, & Rosenthal, 2000;

91 Robert Gerlai, Lee, & Blaser, 2006). Other neuroactive drugs such as cocaine and nicotine were

92 also tested on adult zebrafish and attenuation of swimming activity was observed for both of the

93   two drugs (Draland & Dowling, 2001; Levin, Bencan, & Cerutti, 2007; Lopez-Patino, Yu,
94   Cabral, & Zhdanova, 2008). Furthermore, zebrafish larvae model was studied with same drugs
95   used in adults and mammalians and showed similar behavioural responses (Irons et al., 2010),
96   suggesting that zebrafish larvae are sensitive to neuroactive drugs.
97   However, observations and quantifications of only distance travelled and velocity are not
98   effective in ascertaining the influence of drugs on fish swimming behaviour. Fish swimming
99   kinematics are controlled by consecutive contractions of muscles located along each side of the
100   body, and the muscle contractions are directly driven by motoneurons in the spinal cord, which is
101   part of the central nervous system (CNS) (Ekeberg, Lansner, & Grillner, 1995). The bended body
102   controlled by muscle contractions will interact with the surrounding fluid and change its fluid
103   dynamics to power fish swimming (Voesenek, Muijres, & van Leeuwen, 2018). Under this
104   circumstance, to understand internal muscle mechanics, a useful tool to quantify the association
105   between the effect of drugs on zebrafish swimming behaviour and energetics is required.
106   Although many previous experimental studies managed to visualise fish swimming wake
107   patterns via two-dimensional Particle Image Velocimetry (PIV) flow visualization technique
108   (Muller, 2004; Muller, van den Boogaart, & van Leeuwen, 2008), this is not sufficient to
109   accurately quantify the influences of the drug on fish swimming, which are mainly reflected via
110   muscle mechanical power and force variation. This is a problem that could be potentially solved
111   with a fully coupled fluid structure interaction (FSI) approach between the fish and the
112   surrounding water.
113
114   Inspired by previous work involving Computational Fluid Dynamics (CFD) simulation on fish
115   swimming(Borazjani & Sotiropoulos, 2008, 2009; Carling, Willams, & Bowtell, 1998; J.
116   Lighthill, 1971; Kern & Koumoutsakos, 2006; G. Li, Muller, van Leeuwen, & Liu, 2012), a
117   novel nociception-related zebrafish larva model combining a biological methodology and a CFD
118   simulation analysis tool to quantify drug influences on zebrafish locomotion has been developed
119   and described in this paper. Specifically, we used not only observation of live zebrafish
120   swimming behaviour, but also a CFD simulation tool to quantify a number of important
121   swimming characteristics, including body forces and consumption power, which are hard to
122   acquire with experiments only. In this study, we have studied the influence of particular
123   concentration of diphenylhydantoin (DPH), yohimbine and acetic acid on zebrafish larvae

124   swimming behaviour. The concentration of 500 μM DPH and 100mg/L yohimbine were selected

125   based on previous research as neuroactive drugs in our study (Q. Li et al., 2015; X. Liu et al.,

126   2016). The concentration of 0.01% of acetic acid was selected based on Lopez-Luna's

127   experiment setup (Lopez-Luna, Al-Jubouri, Al-Nuaimy, & Sneddon, 2017b) for a similar

128   pharmacological study including some behavioural studies. In the work of (Peter J. Steenbergen

129   & Bardine, 2014), they compared the levels of cyclooxygenase-2 (cox-2) in zebrafish larvae and

130   found that activation of nociceptive pathways in a low-concentration acetic acid environment

131   produced behavioural changes that were accompanied by changes in levels of cox-2. As the

132   associated gene is involved in nociceptive processes (Bingham, Beswick, Blum, Gray, &

133   Chessell, 2006), it seems reasonable to say that the acid-induced behavioural changes can be

134   attributed to nociception. Therefore, it is appropriate to use acetic acid for nociception study.

135

136   By comparing the forward swimming speed and hydrodynamic power of wild type zebrafish

137   larvae immersed in water, acetic acid, yohimbine hydrochloride solution and 5, 5-

138   diphenylhydantoin sodium salt solution, we demonstrate that our developed analysis tool is able

139   to quantify some differences, such as fish body internal force and energy consumption, between

140   drugs treated group and control group. As the methodology can, to some extent, quantify the

141   differences of internal muscle mechanics before and after drug treatment, this study has

142   established a foundation for studying the effects of new drugs on zebrafish larvae behaviours.

143

144   **2. Materials and Methodology**

145   **2.1. Ethics**

146   Animal work was carried out in compliance with the Animal Ethics and Welfare Committee,

147   Department of Life Sciences, Glasgow Caledonian University, and UK Home Office under

148   Project License PPL 60/4169.

149

150   **2.2. Experiment setup**

151   The experiment setup (**Fig.1A**) and main methodologies were developed in our previous study

152   for the determination of the toxicity of acrylamide on zebrafish locomotion via a colour

153   preference experiment (Jia et al., 2017). In the present study, eighty 5 dpf (days post-

154   fertilization) wildtype zebrafish (Danio rerio) siblings were divided into four groups: the first

155   group (control group) including twenty larvae was immersed in E3 medium (5mM NaCl,

156   0.17mM KCl, 0.33mM CaCl$_2$, 0.22mM MgSO$_4$, and 0.1% methylene blue); the second group

157   including twenty larvae was immersed in E3 medium with 0.01% acetic acid for ten minutes.

158   The third group including twenty larvae was immersed in 500 μM diphenylhydantoin (DPH)

159   solution (5,5-diphenylhydantoin sodium salt) and the fourth group including twenty larvae was

160   immersed in 100mg/L yohimbine solution (yohimbine hydrochloride). The petri dish was

161   illuminated by a light-emitting diode (LED) panel, driven by an adjustable DC power supply

162   (CSI5003XE, Circuit Specialists, and USA) to provide a continuous and constant light. A high-

163   speed video camera (Mikrotron EoSens CL MC1362) was used to record fish swimming

164   behaviour. The frame rate of the camera was set at 500 frames per second (fps) during the entire

165   experiment process. As in the subsequent CFD numerical modelling, the selected fish with a tail

166   beating frequency being less than 70Hz, thus, 7-8 frames within one beat cycle is sufficient to

167   capture the fish tail motion. The water temperature was set at as 27°C as this is the common

168   temperature widely used in zebrafish experiments. Before the camera started recording, fish in

169   all groups were allowed to swim freely for about 10 minutes to adapt to the water environment;

170   once recording started, there was no stimulation to force the fish swimming forward. In this

171   study, only quasi-steady cruising swimming regime is investigated excluding the sudden-start

172   process. This is evident from previous research that cruising with cyclically motion is essential

173   for fish larvae to cover the distance for migration and dispersal (Sancho, Ma, & Lobel, 1997). In

174   addition, cruising swimming has been studied extensively, which makes it easier to compare

175   with other researchers' results.

176

177   **2.3. Data processing algorithm**

178   An in-house *MATLAB* code was developed and used to post-process the recorded videos and

179   extract zebrafish swimming kinematic characteristics, i.e. motion equations. **Figure. 1B** depicts

180   the key steps for the process. The original image recorded from the camera was converted to a

181   binary image consisting of the sketch of zebrafish larva only with "*im2bw*" function in *MATLAB*

182   image processing toolbox. With some adjustments and "*bwboundaries*" function in *MATLAB*, a

183 binary image of zebrafish can be extracted, the entire position vector can be obtained for points

184 distributed on fish outline. All images were skeletonized into a single backbone curve using

185 functions "*bwmorph*" and "*thin*" operation.

186

187 The coordinated pixels on the backbone curve were then divided into equal-distant segments.

188 These segments were simplified as connected straight lines to calculate relative orientation

189 variation with time between two adjacent segments using *MATLAB* curve fitting toolbox.

190 Physical representation of the intersection angle is shown in **Fig. 1C** and the mathematical

191 intersection angle is expressed by **Fig. 1D,** and calculated with Eqn 1, where i denotes the points

192 numbering from one, and θ_j is the relative angle between each two body segments. As

193 elucidated by (Muller, 2004), the travelling wave of curvature travels along the fish body at a

194 near constant rate, thus an averaged frequency was selected for the entire relative orientation

195 functions. Eqn 2 represents a sample prescribed motion equation for relative angle θ_j between

196 each two body segments.

197 $$\theta_j = \arctan(\frac{y_{i+2} - y_{i+1}}{x_{i+2} - x_{i+1}}) - \arctan(\frac{y_{i+1} - y_i}{x_{i+1} - x_i}) \qquad (1)$$

198 $$\theta_j = a\cos(\omega t) + b\sin(\omega t) \qquad (2)$$

199

200 2.4. CFD solver & motion solver

201 2.4.1. Zebrafish larva CFD model

202 Zebrafish larva model used in *OpenFOAM* [22] (https://www.openfoam.com/) was built with 51

203 ellipses extracted from the real fish silhouette and controlled by nine deformation equations as

204 shown in **Fig. 2A.** To simplify the model, the eyes and fin fold are excluded in the CFD fish

205 model. Density of the fish is assumed to be the same as water. The same average body

206 parameters such as body segments mass and length listed in **Table 1** is used for all fish in CFD

207 simulation. The flow field was numerically simulated using the open source CFD toolbox

208 *OpenFOAM* version 3.0.x. The 3-D computational domain is 15 times the fish body length in the

209 longitudinal (x) direction, 10 times of fish body length in transverse (y) direction and 4 times of

210 fish body length in perpendicular (z) direction. The overall fluid domain is assumed to be at rest

211   initially. In the simulation, the medium is water, therefore, the kinematic viscosity of the fluid υ,

212   which can be expressed as $\dfrac{\mu}{\rho}$, is $10^{-6}\,m^2/s$. Pressure boundary conditions are taken as zero

213   gradient for all boundaries except the front and back plane, which are set as symmetry; velocity

214   boundary conditions for fish model were taken as moving wall velocity for all body segments

215   and fixed value for the remaining patches. Local mesh around fish model were depicted in **Fig.**

216   **2B.** Mesh around head region before the vertical dash line shown in **Fig. 2C** is enlarged to be

217   clearer. Considering the constraints in *OpenFOAM* regarding large mesh deformation to model

218   self-propelled zebrafish swimming, fully unstructured mesh was used to tolerate the internal

219   mesh deformation. For ellipses with high aspect ratio, the mesh is specially refined at the tips to

220   ensure that enough cells are present to precisely capture the vortex at the tips. The Reynolds

221   number is defined as $\dfrac{vL}{\upsilon}$, v stands for final constant forward swimming velocity, L is the body

222   length of fish larva, and υ represents the kinematic viscosity. For the entire simulation, Reynolds

223   number is set as 300, which stands for intermediate flow regime.

224

225   **2.4.2. Hydrodynamic solver**

226   To tackle the CFD mesh motion around zebrafish model, a modified *displacementSBRStress*

227   motion solver is applied in *OpenFOAM*. *PimpleDyMFoam* solver is used to solve the transient,

228   incompressible and single-phase Newtonian fluids. *PIMPLE* algorithm, a combination of

229   *SIMPLE* and *PISO*, is used to address velocity-pressure coupling (Y. Liu, Xiao, Incecik, Peyrard,

230   & Wan, 2017). Incompressible laminar Navier-Stokes equation was written in Eqn 3 including

231   the conservation equations of mass and momentum. In this equation, $\vec{U}$ represents the fluid

232   velocity, p is the fluid pressure, ρ is the fluid density, and υ is the fluid kinematic viscosity.

233

234
$$\nabla \cdot (\vec{U}) = 0$$

$$\underbrace{\frac{\partial \vec{U}}{\partial t}}_{time\,accumulation} + \underbrace{\nabla \cdot (\vec{U}\vec{U})}_{convection\,transport} = \underbrace{-\frac{1}{\rho}\nabla p}_{source\,term} + \underbrace{\nabla \cdot (\upsilon\nabla\vec{U})}_{diffusion\,transport} \tag{3}$$

235

236   The time derivatives uses 2nd order implicit discretization scheme, convection term specifies

237   interpolation schemes for velocity as reconCentral, which is different from linear interpolation

238   schemes, it uses extrapolated gradient-based correction from both sides onto the face, using 1/2

239   weighting to increase stability for large deformation.

240

241   In our case, after receiving position and orientation of the body segments from coupled software,

242   *OpenFOAM* will interpolate the boundary displacement of fish body to the entire domain to

243   calculate the internal mesh motion. Forces and moments are calculated by integrating the

244   pressure and skin-friction forces over the patches, they calculated forces include pressure forces

245   and viscous forces, which are parallel and perpendicular to the target patch.

246

247

248   2.4.3. Multibody dynamic software

249

250   The kinematic analysis was based on *MBDyn* [24], a free general purpose multibody dynamics

251   analysis software developed by the department of aerospace engineering of Polytechnic

252   University of Milan (Politecnico di Milano). It solves initial value problem in the form of

253   Differential-Algebraic Equations (DAE), integrated in time domain using A/L-stable multi-step

254   integration schemes (Y. Li, 2014). Constraints can be added independently in *MBDyn*, both for

255   rigid and bended body with six degrees of freedom. As our fish model is not a continuous body

256   and is composed of several rigid body segments, it is convenient to use MBDyn to add multiple

257   constraint equations to control the body deformation. By using reference frame, users are able to

258   specify positions, orientations, linear and angular velocities globally and locally. To be specific,

259   we are able to prescribe the relative body deformation between two adjacent body segments and

260   calculate the forces and power of fish body by coupling with *OpenFOAM*. Dynamics of a set of

261   rigid bodies is written in the form of Newton-Euler equations, constrained by Lagrange's

262   multipliers. For unconstrained nodes, the equations of motion are expressed as

263

264   $M(x)\dot{x} = q$ (4a)

265   $\dot{q} = f(x, \dot{x}, t)$ (4b)

266

267   Where x summarizes the *n* coordinates of the system, M(x) is the mass matrix, q summarizes the

268   momentum and momenta moments, and *f* summarizes the generic force including pressure and

269   viscous force. When the system is subjected to kinematic constraints, the constraints are enforced

270   using Lagrange's multipliers λ, Differential-Algebraic Equations (DAE) are set as:

271

272    $M(x)\dot{x} = q$ (5a)

273    $\dot{q} + \phi^{T}_{/x}\lambda = f(x,\dot{x},t)$ (5b)

274    $\phi(x,t) = 0$ (5c)

275

276   The Differential-Algebraic Equations are integrated with implicit A/L stable linear multistep

277   integration schemes and a prediction-correction approach is used (Masarati, Morandini, &

278   Mantegazza, 2014). In our current case, each body segment was expressed as one node in

279   *MBDyn*. Except the ground node were set as 'static', node, all of the body nodes are dynamic

280   nodes and every two nodes are constrained by a motion equation fitted with *MATLAB* curve-

281   fitting toolbox.

282

283   **2.4.4. Coupling strategy**

284   The above two software are coupled using communication primitives provided by *MBDyn*. To

285   satisfy convergence criteria, a strong coupling, which enables multi-step interactions at each time

286   step, is used between the two software. The schematic diagram for fluid and zebrafish larva

287   motion coupling is shown in **Fig. 2D**. As indicated in **Fig.2D**, kinematic data are transmitted bi-

288   directionally. Inter-process communication is built with Transmission Control Protocol (TCP)

289   socket. An external force element in *MBDyn* allows to communicate positions and orientations of

290   a set of nodes, and the corresponding linear and angular velocities with *OpenFOAM*, the above

291   data can be transmitted either in global frame or in reference frame. On the other side, once

292   kinematic information is received, the forces and moments are calculated based on the changing

293   positions and orientations and transmitted back to *MBDyn*. Once the convergence criteria are

294   satisfied in *OpenFOAM*, *OpenFOAM* stops sending data to *MBDyn*, and forces and moments in

295   the latest step would be used by *MBDyn* and keeps iterating process until convergence. The

296   process is repeated until a final convergent solution is reached.

297

298   3. Results

299   3.1 Validations for multi-body coupling

300   3.1.1 Grid independence & Sensitivity test

301   A grid independence test was carried out on a self-propelled 0.01% acetic acid treated zebrafish

302   model with fully prescribed deformation with two mesh sizes, medium and fine mesh. In

303   addition, the time step influence is also tested, e.g. Case 1: Medium mesh (M) with 83200 total

304   cells and time step of T/650, Case 2: Medium mesh & smaller time step (MS) of 83200 cells and

305   time step of T/1300, and Case 3: Fine mesh (F) of 166400 cells and time step of T/650. The size

306   of the fluid domain remains same for three cases.

307   To exclude mesh resolution and time step size influences on simulation results, we have

308   compared the forward velocity and total force of zebrafish larvae treated with 0.01% acetic acid

309   and the results are shown in **Fig. 3(A-B).** Computational results for three cases including

310   kinematic performance and fluid domain calculation shows close results. To save computational

311   time and keep accuracy, we use the mesh formation and time step size the same as Case1.

312

313   In addition, we have also tested the sensitivity of the results to body segments of zebrafish larvae

314   model with CFD simulation. Considering the accuracy and efficiency for body segmentation, we

315   have divided the body trunk into 5, 10 and 15 segments, respectively. By capturing the body

316   deformation and simulate the forward motion with CFD toolbox, we compared the forward

317   velocity and total hydrodynamic force in **Fig 3(C-D),** indicating that the simulation results are

318   not sensitive to the number of body segments.

319

320

321   3.1.2 Multi-body dynamics validation

322   To validate our numerical coupling methodology on multi-body structure simulation, a

323   comparison based on jellyfish-inspired swimming provided by Wilson was performed (Wilson &

324   Eldredge, 2011). **Fig. 4A** depicts the jellyfish shape, points on the figure indicate how the main

325   body is separated. **Fig. 4B** and **Fig. 4C** illustrate the mathematical model we have created and

326   our CFD model. The prescribed angle functions are represented by θ_1 , θ_2 and θ_3 . Detailed

327   functions are expressed with equations (6). By specifying relative orientation equations between

328   every two sections, the jellyfish model can move upwards with alternant contraction and

329   refilling. Different Reynolds numbers were tested, which is defined by the maximum jellyfish

330   diameter and undulation period, i.e. $\dfrac{D^2_{max}}{T\upsilon}$, D_{max} is the maximum diameter of the jellyfish model,

331   T is the undulation period, and υ denotes kinematic viscosity. Here we selected Re equivalent to

332   140 and 70. **Fig. 5A** and **Fig. 5B** depict the kinematic performance of the multi-body structure

333   with fully prescribed motion, while **Fig. 5C** illustrates the power required for the model to move

334   cyclically and **Fig. 5D** shows the vorticity comparison at Re = 140. All of our results are in close

335   consistent with Wilson & Eldredge's results, the small discrepancies can be caused by the

336   different numerical methods used.

337

338    $\theta_1 =- 0.1472\cos{(6.538t)} - 0.3247\sin{(6.538t)} + 0.7551$

339    $\theta_2 =- 02366\cos{(6.456t)} + 0.1645\sin{(6.456t)} + 0.3472$ (6)

340    $\theta_3 =- 0.08218\cos{(6.427t)} + 0.04095\sin{(6.427t)} + 0.4511$

341

342

343   **3.2. Validations on numerical and experimental methodologies**

344   The first objective of our study was to verify the correctness/accuracy and consistence of

345   proposed experiment and CFD method in this work. To achieve this goal, we used the time-

346   varied angle data, extracted via post-processing of experiment video records as input data to

347   CFD fish body discrete elements, the forward motion of fish is the solution by solving a coupled

348   flow solver and multi-body dynamic method as described in Section 2.4. The first and last fish

349   body segment motion is not prescribed whereas they are our numerical solutions, which

350   represent the fish head and tail locomotion. With simulation results, we first compared our

351   yawing head angle and tail beat angle with data collected from observed zebrafish swimming.

352   **Fig. 6 (A-B)** show an average head and tail angle for 10 individual zebrafish larvae. As seen

353   from the figures, both the head and tail-beat angles were calculated based on the prescribed

354   constrained deformation equations of zebrafish-matched experimentally observed data. Slight

355   differences can be caused by subtle insufficient accuracy of the fish model capturing toolbox,

356   which might lead to slight inconsistency in certain captured points of head/tail angle. The

357   forward swimming velocity shown in **Fig. 6C** reaches about 95% of the experimentally

358   measured swimming speed, approximately 19.25 body lengths per second. The small gap exists

359   as the real fish may not bend the whole body as symmetrically as our model, which is fully

360   controlled by prescribed sinusoidal functions. The subtle modelling errors may additionally lead

361   to differences in swimming speed. We have also calculated the Strouhal number for simulated

362   CFD results. The Strouhal number (St) is defined as $\dfrac{Af}{U}$, where A is the tail beat peak-to-peak

363   amplitude, f is the tail beat frequency and U is the averaged swimming velocity. In our

364   simulation, the Strouhal number is approximately 0.8. A statistical data about forward velocity

365   for 10 zebrafish larvae is shown in **Fig. 6D** (to save space of the image, only ten results are

366   shown).

367

368   **Fig. 7** depicts the vorticity iso-surfaces formed based on Q Criterion behind a swimming normal

369   zebrafish larva at different instants in time within one time period and the dorsal view for

370   vorticity iso-surfaces. Here, Q can describe the wake topology and defines vortices as positive

371   second invariant of velocity gradient in region where vorticity magnitude is greater than strain-

372   rate magnitude (Kolář, 2007). As seen from the most left and right column of **Fig. 7**, flow

373   patterns behind the fish are represented by detached vortices and shown as translucent green

374   fragments. Vortices starts to form in the vicinity of head, transmits downstream to tail and

375   detaches at the tail, which are consistent with the fish tail motion; when the lateral displacement

376   of the tail reaches the highest amplitude, vortices starts to shed at the tail tip, the already formed

377   vorticity in the wake are mixed with the newly formed vorticity at tail tip. The most right column

378   also displays a 3-D view of the vortex rings generated behind the fish to understand formation of

379   flow patterns better. To validate the numerical methodology, **Fig. 7** also compares the body

380   curvatures of CFD model and the real fish in the recorded experiment video. As can be seen, two

381   sets of results match very well in terms of body shape at all specific time within a period,

382   indicating that our CFD model is able to imitate the self-propelled swimming of zebrafish larva

383   and its interactions with surrounding fluid.

384

385   **3.3. Power distribution along fish body and an initial approximation of the cost of**

386   **transport**

387   As the movement of each two neighbouring body segments is constrained with a prescribed

388   deformation equation except for fish head and tail, mechanical power distribution along the fish

389   body can be approximated by power generated by each body segment. The mechanical power

390   generated from fish muscle includes the translational power due to linear motion and the

391   rotational power due to body rotation. As the fish is moving cyclically, all the other terms are

392   cancelled out except for the rotational power. Therefore, the mechanical power is estimated with

393   the cross product of torque and angular velocity shown as equation 7(a), and the total power

394   transmitted into the water is calculated with equation 7(b).

395
396

397    $$P_M = \sum_i M_i \cdot \omega_i \qquad\qquad\qquad 7(a)$$

398

399    $$P_H = \sum_j -F_j \cdot V_j \qquad\qquad\qquad 7(b)$$

400
401    $$\overline{P_M} = \overline{P_H} \qquad\qquad\qquad 7(c)$$

402

403   In the above equation, P_M is the mechanical power of fish muscle, and P_H represents

404   hydrodynamic power generated by interactions with surrounding fluid. M_i is the internal torque

405   for the ith joint calculated by MBDyn in the global frame, ω_i represents the angular velocity for

406   the ith joint. F_j is the hydrodynamic force acting on the jth body and V_j represents the jth body

407   velocity.

408
409   During muscle contraction, fish body bends, energy is generated and transmitted into the water,

410   and the bended body interacts with the surrounding fluid, a thrust force generates and pushes the

411   fish moving forward. Within this process, Approximately 20% of the energy (depending on fish

412   species, the percentage can float dramatically) (Zhang, Yu, & Tong, 2014) generated by muscle

413   contraction is consumed due to the viscous dissipation of fish body tissues, and the remaining

414   energy is transmitted into the water. In our model, viscous dissipations of fish body tissues are

415   neglected to simplify the simulation. Therefore, as the variation of kinetic energy is zero during

416   cyclic swimming, the mechanical power is fully transformed into the hydrodynamic power,

417   which means the absolute value hydrodynamic power equals the mechanical power, and we only

418   need to show hydrodynamic power for 20 zebrafish larvae as depicted in **Fig. 8B**. The calculated

419   hydrodynamic power has been changed into absolute values as the sign is different from

420   mechanical power. To further understand the different power generated at different locations

421   along the fish body, we have compared the time-history of forces and velocity in **Fig. 8** at three

422   typical points shown in **Fig. 8A**, representing head region, body region and tail region. The

423   trajectory is not completely parallel to x axis in global frame, force and velocity shown in **Fig.**

424   **8C** and **Fig. 8D** are pointing towards the real moving direction of zebrafish. An approximation of

425   hydrodynamic power distribution on each body section is also depicted. As shown in **Fig. 8E**, the

426   averaged hydrodynamic power for 20 fish larvae shows a significant higher value starting from

427   approximately 75% of body length. According to motion equations, this region has the largest

428   motion amplitude along the body in global frame, resulting in larger fluid force, thus more

429   hydrodynamic power. In **Fig. 8F**, the mechanical power generated along the body shows an

430   increase towards the tail and a steep decrease at the tail.

431

432   Detailed mechanical and hydrodynamic power and an approximation of cost of transport are

433   summarised in **Table 2.** The cost of transport is defined as energy spent to travel unit distance

434   per unit mass, which is expressed as $\dfrac{P_m}{U}$, P_m is the power per unit mass, and U is the forward

435   velocity. Limited by the size of the table, only ten fish data was selected and displayed in the

436   table.

437   **3.4. Comparison of kinematics and energetics between normal group and drug treated**

438   **groups**

439   Swimming performance of zebrafish larvae might be affected by drugs with different

440   concentrations. According to Lopez-Luna's research (Lopez-Luna et al., 2017b), zebrafish larvae

441   exposed to 0.01% acetic acid displayed more active responses than the normal zebrafish, and

442 these active behaviours were sustained for longer. Liu has tested influences of diphenylhydantoin

443 (DPH) on 5 dpf zebrafish larvae locomotion at different concentrations and found that exposure

444 to higher concentrations of DPH under light condition leads to decreased locomotor activities (X.

445 Liu et al., 2016). Their team also tested the effect of 100mg/L yohimbine on 5 dpf zebrafish

446 larvae, but no obvious effect has been found on locomotor activity under light condition (Q. Li et

447 al., 2015). By simulating the swimming behaviours of zebrafish larvae under these circumstance,

448 we examined the forward swimming velocity and cost of transport differences after exposing to

449 0.01% acetic acid, 500 μM DPH, and 100 mg/L yohimbine. **Fig. 9A** and **Fig. 9D** depict the

450 averaged head and tail comparison for three drugs and control group zebrafish larvae. As the

451 different frequencies and initial angles were used, phase differences existed among those groups

452 in head and tail angle respectively. From the figure, there are no significant differences for the

453 amplitude of head angle, whereas the maximum tail beat angle for zebrafish larva immersed in

454 the 0.01% acetic acid showed a larger value compared with the rest groups. **Fig. 9B** illustrates

455 the forward swimming speed comparison between control group zebrafish and drug treated

456 groups. The forward velocity for acetic acid treated zebrafish is dramatically higher than other

457 groups' zebrafish, but there is no significant differences between control group and yohimbine

458 treated group. For zebrafish treated with 500 μM DPH solution, there is a significant decrease of

459 velocity compared with other groups. These results indicate that the forward swimming velocity

460 might be influenced by the body undulation frequency and tail beat amplitude. With larger

461 frequency and tail beat amplitude being represented by maximum tail beat angle, the forward

462 swimming speed tended to increase.

463

464 As the tail beat frequency and amplitude are both increased, energy generated by fish body will

465 increase as well, which might give rise to lower efficiency as the side oscillations consumes

466 more energy without contributions to thrust. **Fig. 9C** displays comparisons of the hydrodynamic

467 power P_H, cost of transport were calculated for all cases, resulting in $81.73 \mu J / m \cdot kg$,

468 $96.24 \mu J / m \cdot kg$, $65.44 \mu J / m \cdot kg$ and $82.32 \mu J / m \cdot kg$ for control, acetic acid treated, DPH

469 treated, and yohimbine treated group, respectively. These values are similar to those reported by

470 Li et al. (from $105 \mu J / m \cdot kg$ to $50 \mu J / m \cdot kg$ in (G. Li, Muller, van Leeuwen, & Liu, 2016)) on

471 larval zebrafish. It appears that the DPH treated group performed with greater efficiency than the

472 other groups as it has the lowest tail beat amplitude and frequency. **Fig. 9E** depicts the forward

473 velocity for all groups. Based on the assumption of no differences among those groups, we have

474 calculated the P value, which is usually evaluated in statistical hypothesis testing to determine

475 the reliability of the results. The P value is smaller than 0.0001 for control group comparison

476 with DPH treated group and acetic acid treated group, which indicates that significant increment

477 of forward velocity can be seen after 0.01 % acetic acid treatment, and a decrease of velocity

478 happens after treated with 500 μM DPH solution. There is no obvious differences between

479 control group and yohimbine treated group, indicating that 100mg/L concentration of yohimbine

480 will not influence the locomotion behaviour dramatically of 5 dpf zebrafish larvae. **Fig. 9F**

481 displays similar comparison as **Fig. 9E**, but with the parameter changed to hydrodynamic power.

482 The resulting P value is smaller than 0.0001 for control group comparison with DPH treated

483 group and acetic acid treated group, leading to the conclusion that averaged hydrodynamic power

484 of acetic acid treated zebrafish larvae is higher than the control group specimens, whereas the

485 zebrafish larvae treated with DPH solution resulted in lower averaged hydrodynamic power.

486 There is no obvious difference between control group and yohimbine treated group as well,

487 which is consistent with results shown in **Fig. 9E**. **Fig. 10** compares the vorticity on x-y plane of

488 the 3-D fish model. By comparing them in one period of time, it can be seen that the vortex

489 detached from the tail tip is faster for acid treated group compared with control group fish. The

490 earlier detached vortex has been labelled with black circles in the right column, indicating the

491 larger distance travelled within one period of time, i.e., higher velocity. For DPH treated group,

492 within same one period of time, the evolution of vorticity is much shorter than other groups,

493 approximately half of other groups, suggesting that only half of the distance travelled by DPH

494 treated group compared with control group. For yohimbine treated group, vorticity patterns are

495 similar to those in control group. All of the vorticity results for drug treated groups are in

496 consistent with velocity comparisons depicted in **Fig.9**.

497

4. Discussions

499 A novel methodology connecting biological experiments and CFD simulation to explore the

500 relationship between zebrafish larvae fish swimming behaviour and intravital body force/torque

501 changes is proposed and tested in this study. By using the observed zebrafish locomotion, we

502 extracted the kinematic swimming equations and entered them into our numerical modelling tool

503 to achieve a fluid-body interaction numerical simulation. Although the estimated final cyclic

504 averaged swimming speed of zebrafish larvae via CFD is slightly lower than the experimentally

505 observed results, overall agreement between experiment and CFD is acceptable. Compared with

506 previous studies on zebrafish larvae (G. Li et al., 2012; G. Li et al., 2016), the resultant

507 swimming motion and energetics are within a reasonable range. The estimated Strouhal number

508 is around 0.8, which is much higher than optimal streamlined fish swimming value of 0.5, the

509 probable reason might be due to that the zebrafish larvae swims in intermediate flow regime

510 where viscous force dominant, Therefore, overcoming such viscous effect requires more thrust

511 and thus higher Strouhal number is needed (Voesenek et al., 2018). As shown in Fig 7, though

512 we can conclude some differences from the stage of vortex detach by comparing the vorticity in

513 the wake that can be acquired from experimental observations, distinctions between control and

514 acetic treated group are still not clear, which might require quantified data from CFD results

515 described in the previous paragraphs to further identify the differences, indicating the potentials

516 of CFD simulation in the comparisons of nociceptive related studies.

517

518 We have also calculated the hydrodynamic power distribution along the body as shown in **Fig**

519 **5E**. Based on our results, the hydrodynamic power generation shows an increase starting from

520 the centre of mass and a steep increase in the rear region. Ideally, the consumption of muscle

521 power requires a study of muscle strain and electromyography (EMG) patterns for muscle

522 function at specific positions along the body; however, the extremely small body size of larval

523 fish makes it impossible to place receivers on the body. Constraints added in our fish model

524 provide energy to move forward from static state, which perform as muscle fibre in real fish to

525 provide mechanical power. Mechanical power distribution has been examined in **Fig 5F**,

526 showing a steep increase towards the tail from the middle region and then a steep decrease in the

527 tail region. This might suggest that the main power generated by muscle to support steady

528 forward swimming exists in the entire body. The conclusion seems to be inconsistent with the

529 previous viewpoint that most power is generated in the anterior region, while the posterior region

530 performs like a transmitter. However, based on the equations set up in our model, the anterior

531 region equations have smaller curvature, implying that the simulated muscle in this region has

532 smaller strain when it is contracted, thus less positive work is done. Moreover, during steady

533   swimming state, red muscle dominates the swimming motion; if the main muscle power is

534   generated in the anterior part, loss of energy in the form of heat occurs in the process of force

535   transmission towards the tail, which might increase the burden of red muscle as it powers the

536   entire steady swimming process (Rome, Swank, & Corda, 1993). Given that muscle functions

537   vary among different species, our results need to be further tested with the help of biological

538   analysis.

539

540   Acetic acid treated zebrafish might accelerate quicker, i.e., higher frequency, to reach the

541   maximum speed as it attempts to escape the acid environment (Lopez-Luna et al., 2017a). Our

542   results show that the acid treated group achieved higher tail beat frequency and swimming speed

543   than control group. The increment of speed in the intermediate flow regime ($10<Re<10^3$)

544   increased the energy dissipation, resulting in higher cost of transport, which agrees with previous

545   study by Li et al. (2012).

546

547   Two neuroactive drugs used in this paper, diphenylhydantoin (DPH) and yohimbine are both

548   sensitive to zebrafish larvae, for different days of post fertilization, behavioural changes are

549   different. (Irons et al., 2010). Besides, different concentrations and lighting conditions can cause

550   reversed results for same drug. For example, for 5 dpf zebrafish larvae, 10 mg/L yohimbine will

551   increase the locomotion activity of fish larvae, whereas 200 mg/L yohimbine will decrease the

552   activity. In our study, 5 dpf zebrafish larvae applied with 500 μM DPH and 100mg/L yohimbine

553   lead to similar results compared with previous biological observations (Q. Li et al., 2015; X. Liu

554   et al., 2016), indicating that our method has the ability to replicate neuroactive drug influences

555   on zebrafish larvae locomotion behaviours. The effect of exposure to acid on zebrafish

556   swimming behaviour has been studied for different substances including acetic acid and citric

557   acid and at different zebrafish developmental stages (Lopez-Luna et al., 2017a; Nordgreen,

558   Tahamtani, Janczak, & Horsberg, 2014). However, these studies were limited to the nociceptive

559   responses of zebrafish larvae on stress, fear or anxiety, i.e. environment influences. Furthermore,

560   the observed data mainly focused on the total distance fish travelled in a period of time or the

561   time spent in active status(Lopez-Luna et al., 2017a, 2017b). To some extent, our developed tool

562   can mimic the mutual interactions of real fish with the surrounding fluid and thus allows

563   investigation of the relationship between fish body mechanical force and torque and its

564 swimming behaviours. Using this approach, our future work would focus on evaluating potential
565 analgesic drugs for pain relief and neuroactive drug effects on fish behaviours, which might help
566 to understand functions of nervous system.

567

568 A possible factor that might influence the accuracy of our results is the fish body stiffness, which
569 has not been taken into account in the present research but has been studied by other groups.
570 (McHenry & van Netten, 2007) Studied the flexural stiffness of superficial neuromasts as it is
571 correlated with the detection of surrounding fluid. Zhang, et al (Zhang, et al,. 2014) provided a
572 prediction of fish body's visco-elastic properties and related muscle mechanical behaviour *in*
573 *vivo* based on a continuous beam model (Zhang et al., 2014). Real fish are able to adjust their
574 body stiffness at specific positions in order to optimize their swimming performance such as the
575 maximum forward speed and minimum energy cost (Eric D. Tytell et al., 2016). However, the
576 distribution of visco-elastic properties, i.e. stiffness and damping coefficients along the fish
577 body, are difficult to measure precisely, thus the mutual contributions from visco-elastic
578 properties to the optimized swimming performance cannot be determined individually.
579 Moreover, it is technically difficult to observe subtle body curvature changes. Different fish
580 species may have different stiffness and damping characteristics for different purposes, such as
581 for acceleration/deceleration or cruising swimming (Eric D. Tytell, Hsu, & Williams, 2010).
582 Considering the importance of body stiffness for a better understanding of muscle functions in
583 controlling fish swimming, we intend to focus in our future research on the visco-elastic
584 properties at some predicted positions with the help of muscle dissection. To be specific, muscle
585 related adverse medical treatment may have effects on muscle tissues such as shortened or
586 dissolved local muscle fibres (Lin, 2012). By applying predicted stiffness and damping
587 coefficients and comparing these with the live fish tissue properties at those locations, it might be
588 possible to account for the influences on altered swimming behaviours.

589

590 **5. Conclusions**

591 In this paper, a novel method has been introduced to quantify the influence of drugs on zebrafish
592 locomotion kinematics and energetics. Experimental results have compared with CFD simulated
593 results on tail beat angle and forwards velocity and showed consistent values. Three types of
594 drugs with positive effect, negative effect and no effect on zebrafish locomotion activity

595   validated by previous researches have been applied to study applications of our methodology.

596   Reasonable comparison results have been supplied, 0.01% acetic acid has a positive influence on

597   5 dpf zebrafish locomotion, 500 μM diphenylhydantoin solution has a negative effect on

598   zebrafish locomotion, and the 100mg/mL yohimbine will not influence swimming behaviours of

599   5 dpf zebrafish larvae significantly. We have also provide results related to internal muscle

600   mechanics, including power distribution along the body and hydrodynamic power comparison,

601   providing insights into internal muscle influences on fish swimming.

602

603   There are still some questions to be solved related to this direction, particularly with respect to

604   how the change of internal muscle could influence swimming behaviours of zebrafish larvae, and

605   how the passive control of fish muscle contributes to swimming efficiency. Evaluation of the

606   analgesic and neuroactive drugs on fish behaviours is also an ongoing effort.

607

608   Acknowledgements

609   This work was supported by laboratory of Department of Biological and Biomedical Sciences in

610   Glasgow Caledonia University. We thank the support from Dr Gen Li and Professor Hao Liu on

611   reviewing the manuscript and apparatus provided by Dr Xinhua Shu for zebrafish experiment.

612

613   Author Disclosure Statement

614   No competing financial interests exist.

615

616

617

618

References

Anderson, K. V., & Ingham, P. W. (2003). The transformation of the model organism: a decade of developmental genetics. *Nat Genet, 33 Suppl*, 285-293. Retrieved from https://www.ncbi.nlm.nih.gov/pubmed/12610538. doi:10.1038/ng1105

Bingham, S., Beswick, P. J., Blum, D. E., Gray, N. M., & Chessell, I. P. (2006). The role of the cylooxygenase pathway in nociception and pain. *Semin Cell Dev Biol, 17*(5), 544-554. Retrieved from http://www.ncbi.nlm.nih.gov/pubmed/17071117. doi:10.1016/j.semcdb.2006.09.001

Borazjani, I., & Sotiropoulos, F. (2008). Numerical investigation of the hydrodynamics of carangiform swimming in the transitional and inertial flow regimes. *The Journal of Experimental Biology, 211*(Pt 10), 1541-1558. Retrieved from http://www.ncbi.nlm.nih.gov/pubmed/18456881. doi:10.1242/jeb.015644

Borazjani, I., & Sotiropoulos, F. (2009). Numerical investigation of the hydrodynamics of anguilliform swimming in the transitional and inertial flow regimes. *The Journal of Experimental Biology, 212*(Pt 4), 576-592. Retrieved from http://www.ncbi.nlm.nih.gov/pubmed/19181905. doi:10.1242/jeb.025007

Carling, J., Willams, T. L., & Bowtell, G. (1998). Self-propelled anguilliform swimming: simulations solution of the two-dimensional navier-stokes equations and newton's laws of motion. *The Journal of Experimental Biology, 201*, 24.

Correia, A. D., Cunha, S. R., Scholze, M., & Stevens, E. D. (2011). A Novel Behavioral Fish Model of Nociception for Testing Analgesics. *Pharmaceuticals, 4*(4), 665-680. doi:10.3390/ph4040665

Dlugos, C. A., & Rabin, R. A. (2003). Ethanol effects on three strains of zebrafish: model system for genetic investigations. *Pharmacology, Biochemistry and Behavior, 74*, 10.

Draland, T., & Dowling, J. E. (2001). Behavioral screening for cocaine sensitivity in mutagenized zebrafish *PNAS, 98*, 6.

Ekeberg, O., Lansner, A., & Grillner, S. (1995). The Neural Control of Fish Swimming Studied Through Numerical Simulation. *Adaptive Behavior, 3*.

Gerlai, R., Lahav, M., Guo, S., & Rosenthal, A. (2000). Drinks like a fish: zebra fish (Danio rerio) as a behavior genetic model to study alcohol effects. *Pharmacology, Biochemistry and Behavior, 67*, 10.

Gerlai, R., Lee, V., & Blaser, R. (2006). Effects of acute and chronic ethanol exposure on the behavior of adult zebrafish (Danio rerio). *Pharmacology Biochemistry and Behavior, 85*, 18.

Gregory, N. S., Harris, A. L., Robinson, C. R., Dougherty, P. M., Fuchs, P. N., & Sluka, K. A. (2013). An overview of animal models of pain: disease models and outcome measures. *J Pain, 14*(11), 1255-1269. Retrieved from http://www.ncbi.nlm.nih.gov/pubmed/24035349. doi:10.1016/j.jpain.2013.06.008

Irons, T. D., MacPhail, R. C., Hunter, D. L., & Padilla, S. (2010). Acute neuroactive drug exposures alter locomotor activity in larval zebrafish. *Neurotoxicology and Teratology, 32*(1), 84-90. doi:10.1016/j.ntt.2009.04.066

J. Lighthill, M. (1971). *Large-Amplitude Elongated-Body Theory of Fish Locomotion* (Vol. 179).

661 Jia, L., Raghupathy, R. K., Albalawi, A., Zhao, Z., Reilly, J., Xiao, Q., & Shu, X. (2017). A colour
662   preference technique to evaluate acrylamide-induced toxicity in zebrafish. *Comp Biochem*
663   *Physiol   C   Toxicol   Pharmacol,   199*,   11-19.   Retrieved   from
664   http://www.ncbi.nlm.nih.gov/pubmed/28111251. doi:10.1016/j.cbpc.2017.01.004
665 Kern, S., & Koumoutsakos, P. (2006). Simulations of optimized anguilliform swimming. *The*
666   *Journal   of   Experimental   Biology,   209*(Pt   24),   4841-4857.   Retrieved   from
667   http://www.ncbi.nlm.nih.gov/pubmed/17142673. doi:10.1242/jeb.02526
668 Kolář, V. (2007). Vortex identification: New requirements and limitations. *International Journal*
669   *of Heat and Fluid Flow, 28*(4), 638-652. doi:10.1016/j.ijheatfluidflow.2007.03.004
670 Levin, E. D., Bencan, Z., & Cerutti, D. T. (2007). Anxiolytic effects of nicotine in zebrafish. *Physiol*
671   *Behav, 90*(1), 54-58. Retrieved from https://www.ncbi.nlm.nih.gov/pubmed/17049956.
672   doi:10.1016/j.physbeh.2006.08.026
673 Li, F., Lin, J., Liu, X., Li, W., Ding, Y., Zhang, Y., . . . Li, Q. (2018). Characterization of the locomotor
674   activities of zebrafish larvae under the influence of various neuroactive drugs. *Ann Transl*
675   *Med, 6*(10), 173. Retrieved from https://www.ncbi.nlm.nih.gov/pubmed/29951495.
676   doi:10.21037/atm.2018.04.25
677 Li, G., Muller, U. K., van Leeuwen, J. L., & Liu, H. (2012). Body dynamics and hydrodynamics of
678   swimming fish larvae: a computational study. *The Journal of Experimental Biology, 215*(Pt
679   22), 4015-4033. Retrieved from http://www.ncbi.nlm.nih.gov/pubmed/23100489.
680   doi:10.1242/jeb.071837
681 Li, G., Muller, U. K., van Leeuwen, J. L., & Liu, H. (2016). Fish larvae exploit edge vortices along
682   their dorsal and ventral fin folds to propel themselves. *J R Soc Interface, 13*(116).
683   Retrieved   from   http://www.ncbi.nlm.nih.gov/pubmed/27009180.
684   doi:10.1098/rsif.2016.0068
685 Li, Q., Lin, J., Zhang, Y., Liu, X., Chen, X. Q., Xu, M. Q., . . . Guo, N. (2015). Differential behavioral
686   responses of zebrafish larvae to yohimbine treatment. *Psychopharmacology (Berl),*
687   *232*(1), 197-208. Retrieved from https://www.ncbi.nlm.nih.gov/pubmed/24958231.
688   doi:10.1007/s00213-014-3656-5
689 Li, Y. (2014). Coupled Computational fluid dynamics/multibody dynamics method with
690   application to wind turbine simulations. *Lowa Research online*.
691 Lin, Y. Y. (2012). Muscle diseases in the zebrafish. *Neuromuscul Disord, 22*(8), 673-684. Retrieved
692   from http://www.ncbi.nlm.nih.gov/pubmed/22647769. doi:10.1016/j.nmd.2012.04.007
693 Liu, X., Lin, J., Zhang, Y., Peng, X., Guo, N., & Li, Q. (2016). Effects of diphenylhydantoin on
694   locomotion and thigmotaxis of larval zebrafish. *Neurotoxicol Teratol, 53*, 41-47. Retrieved
695   from https://www.ncbi.nlm.nih.gov/pubmed/26597863. doi:10.1016/j.ntt.2015.11.008
696 Liu, Y., Xiao, Q., Incecik, A., Peyrard, C., & Wan, D. (2017). Establishing a fully coupled CFD analysis
697   tool for floating offshore wind turbines. *Renewable Energy, 112*, 280-301.
698   doi:10.1016/j.renene.2017.04.052
699 Lopez-Luna, J., Al-Jubouri, Q., Al-Nuaimy, W., & Sneddon, L. U. (2017a). Impact of stress, fear and
700   anxiety on the nociceptive responses of larval zebrafish. *PLOS one, 12*(8), e0181010.
701   Retrieved   from   http://www.ncbi.nlm.nih.gov/pubmed/28767661.
702   doi:10.1371/journal.pone.0181010
703 Lopez-Luna, J., Al-Jubouri, Q., Al-Nuaimy, W., & Sneddon, L. U. (2017b). Reduction in activity by
704   noxious chemical stimulation is ameliorated by immersion in analgesic drugs in zebrafish.

705   *The Journal of Experimental Biology, 220*(Pt 8), 1451-1458. Retrieved from
706   http://www.ncbi.nlm.nih.gov/pubmed/28424313. doi:10.1242/jeb.146969

707 Lopez-Patino, M. A., Yu, L., Cabral, H., & Zhdanova, I. V. (2008). Anxiogenic effects of cocaine
708   withdrawal in zebrafish. *Physiol Behav, 93*(1-2), 160-171. Retrieved from
709   https://www.ncbi.nlm.nih.gov/pubmed/17889042. doi:10.1016/j.physbeh.2007.08.013

710 Malafoglia, V., Bryant, B., Raffaeli, W., Giordano, A., & Bellipanni, G. (2013). The zebrafish as a
711   model for nociception studies. *J Cell Physiol, 228*(10), 1956-1966. Retrieved from
712   http://www.ncbi.nlm.nih.gov/pubmed/23559073. doi:10.1002/jcp.24379

713 Malafoglia, V., Colasanti, M., Raffaeli, W., Balciunas, D., Giordano, A., & Bellipanni, G. (2014).
714   Extreme thermal noxious stimuli induce pain responses in zebrafish larvae. *J Cell Physiol,*
715   *229*(3), 300-308. Retrieved from http://www.ncbi.nlm.nih.gov/pubmed/23929528.
716   doi:10.1002/jcp.24447

717 Masarati, P., Morandini, M., & Mantegazza, P. (2014). An Efficient Formulation for General-
718   Purpose Multibody/Multiphysics Analysis. *Journal of Computational and Nonlinear*
719   *Dynamics, 9*(4), 041001. doi:10.1115/1.4025628

720 McHenry, M. J., & van Netten, S. M. (2007). The flexural stiffness of superficial neuromasts in the
721   zebrafish (Danio rerio) lateral line. *J Exp Biol, 210*(Pt 23), 4244-4253. Retrieved from
722   http://www.ncbi.nlm.nih.gov/pubmed/18025022. doi:10.1242/jeb.009290

723 Mettam, J. J., McCrohan, C. R., & Sneddon, L. U. (2012). Characterisation of chemosensory
724   trigeminal receptors in the rainbow trout, Oncorhynchus mykiss: responses to chemical
725   irritants and carbon dioxide. *J Exp Biol, 215*(Pt 4), 685-693. Retrieved from
726   http://www.ncbi.nlm.nih.gov/pubmed/22279076. doi:10.1242/jeb.060350

727 Muller, U. K. (2004). Swimming of larval zebrafish: ontogeny of body waves and implications for
728   locomotory development. *The Journal of Experimental Biology, 207*(5), 853-868.
729   doi:10.1242/jeb.00821

730 Muller, U. K., van den Boogaart, J. G., & van Leeuwen, J. L. (2008). Flow patterns of larval fish:
731   undulatory swimming in the intermediate flow regime. *The Journal of Experimental*
732   *Biology, 211*(Pt 2), 196-205. Retrieved from
733   http://www.ncbi.nlm.nih.gov/pubmed/18165247. doi:10.1242/jeb.005629

734 Nordgreen, J., Tahamtani, F. M., Janczak, A. M., & Horsberg, T. E. (2014). Behavioural effects of
735   the commonly used fish anaesthetic tricaine methanesulfonate (MS-222) on zebrafish
736   (Danio rerio) and its relevance for the acetic acid pain test. *PLOS one, 9*(3), e92116.
737   Retrieved from http://www.ncbi.nlm.nih.gov/pubmed/24658262.
738   doi:10.1371/journal.pone.0092116

739 Peter J. Steenbergen, & Bardine, N. (2014). Antinociceptive effects of buprenorphine in zebrafish
740   larvae: An alternative for rodent models to study pain and nociception? *Applied Animal*
741   *Behaviour Science, 152*, 92-99.

742 Rome, L. C., Swank, D., & Corda, D. (1993). How Fish Power Swimming *Science, 261*(5119), 4.

743 Roques, J. A., Abbink, W., Geurds, F., van de Vis, H., & Flik, G. (2010). Tailfin clipping, a painful
744   procedure: Studies on Nile tilapia and common carp. *Physiol Behav, 101*(4), 533-540.
745   Retrieved from http://www.ncbi.nlm.nih.gov/pubmed/20705079.
746   doi:10.1016/j.physbeh.2010.08.001

747 Sancho, G., Ma, D., & Lobel, P. (1997). Behavioral observations of an upcurrent reef colonization
748   event by larval surgeonfish Ctenochaetus strigosus (Acanthuridae). *Marine Ecology*
749   *Progress Series, 153*, 311-315. doi:10.3354/meps153311
750 Sison, M., Cawker, J., Buske, C., & Gerlai, R. (2006). Fishing for genes influencing vertebrate
751   behavior: zebrafish making headway. *Lab Animal, 35*(5), 33-39. Retrieved from
752   https://doi.org/10.1038/laban0506-33. doi:10.1038/laban0506-33
753 Taylor, J. C., Dewberry, L. S., Totsch, S. K., Yessick, L. R., DeBerry, J. J., Watts, S. A., & Sorge, R. E.
754   (2017). A novel zebrafish-based model of nociception. *Physiol Behav, 174*, 83-88.
755   Retrieved from http://www.ncbi.nlm.nih.gov/pubmed/28288793.
756   doi:10.1016/j.physbeh.2017.03.009
757 Tytell, E. D., Hsu, C.-Y., & Williams, T. L. (2010). Interactions between internal forces, body
758   stiffness, and fluid environment in a neuromechanical model of Lamprey swimming.
759   *Biophyics and Computational Biology*. doi:10.1073/pnas.1011564107/-/DCSupplemental
760 Tytell, E. D., Leftwich, M. C., Hsu, C.-Y., Griffith, B. E., Cohen, A. H., Smits, A. J., . . . Fauci, L. J.
761   (2016). Role of body stiffness in undulatory swimming: Insights from robotic and
762   computational models. *Physical Review Fluids, 1*(7). doi:10.1103/PhysRevFluids.1.073202
763 Voesenek, C. J., Muijres, F. T., & van Leeuwen, J. L. (2018). Biomechanics of swimming in
764   developing larval fish. *J Exp Biol, 221*(Pt 1). Retrieved from
765   https://www.ncbi.nlm.nih.gov/pubmed/29326114. doi:10.1242/jeb.149583
766 Wilson, M. M., & Eldredge, J. D. (2011). Performance improvement through passive mechanics
767   in jellyfish-inspired swimming. *International Journal of Non-Linear Mechanics, 46*(4), 557-
768   567. doi:10.1016/j.ijnonlinmec.2010.12.005
769 Xi, Y., Ryan, J., Noble, S., Yu, M., Yilbas, A. E., & Ekker, M. (2010). Impaired dopaminergic neuron
770   development and locomotor function in zebrafish with loss of pink1 function. *Eur J*
771   *Neurosci, 31*(4), 623-633. Retrieved from
772   https://www.ncbi.nlm.nih.gov/pubmed/20141529. doi:10.1111/j.1460-
773   9568.2010.07091.x
774 Zhang, W., Yu, Y., & Tong, B. (2014). Prediction of fish body's passive visco-elastic properties and
775   related muscle mechanical performance in vivo during steady swimming. *Science China*
776   *Physics, Mechanics and Astronomy, 57*(2), 354-364. doi:10.1007/s11433-013-5372-2
777

Figure 1

Experimental method used to extract zebrafish motion equations

(A) Experiment apparatus for zebrafish swimming video recording. High speed camera is used to capture the fish motion in petri dish (B) zebrafish image extracted from one frame of the video (C) zebrafish outline expressed with white curve and central of mass expressed with green dot (D) zebrafish backbone expressed with white line (E) Equal-distant divisions of the backbone curve, divided with several green dots (F) Expression of relative angle between two segments (G) Intesection angle calculation between each two segments along the backbone.
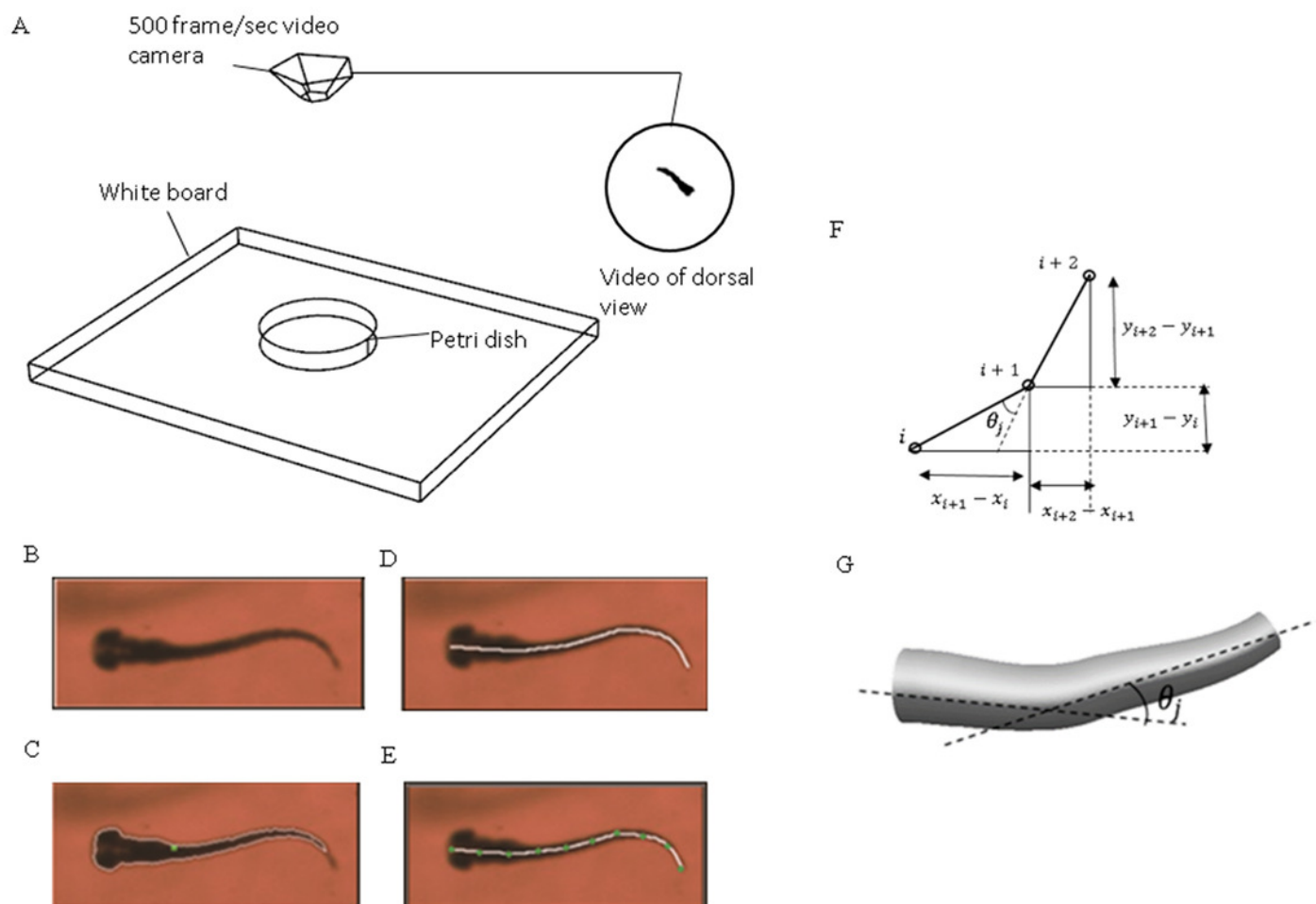
Figure 2

CFD simulation procedure and mesh geometry of the fish

(A) Flow chart of data transmission between OpenFOAM and MBDyn. Force and displacement vectors are transmitted between OpenFOAM and MBDyn (B) CAD geometry of fish body. The fish body composes of 51 ellipses with different aspect ratio fish body is divided into nine sections with black hollow circle (C) local mesh on fish body in CFD. To accommodate the local mesh rotation and translation, unstructured mesh is built around fish body (D) Enlarged mesh formation around fish head region
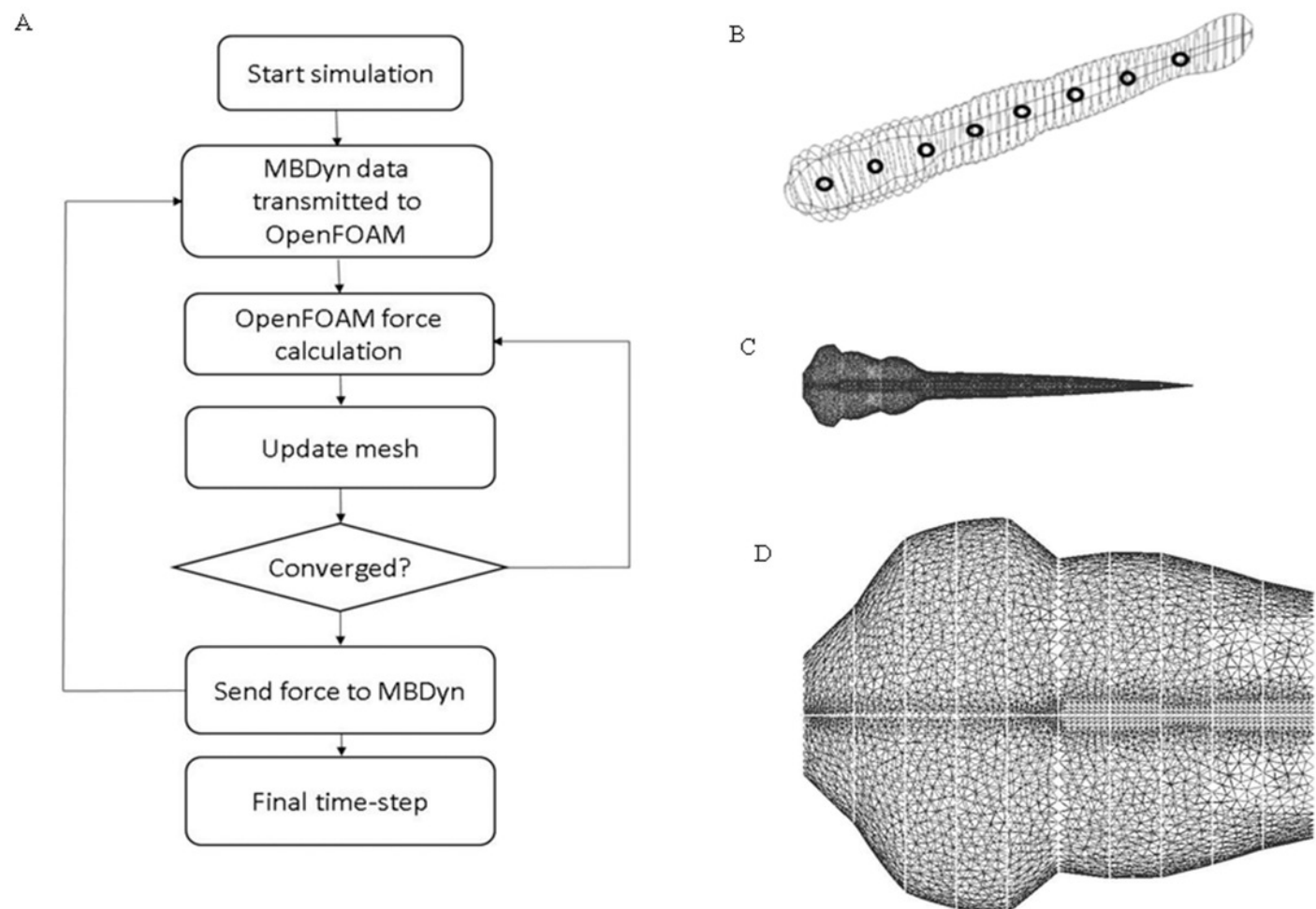
Figure 3

Grid independence test with acetic acid treated zebrafish larva sensitivity study

(A) Forward velocity for three levels of grid. (B) Total force in the moving direction for three levels of grid. (C) Forward velocity for three numbers of segmentations. (D) Total hydrodynamic force for three numbers of segmentations.
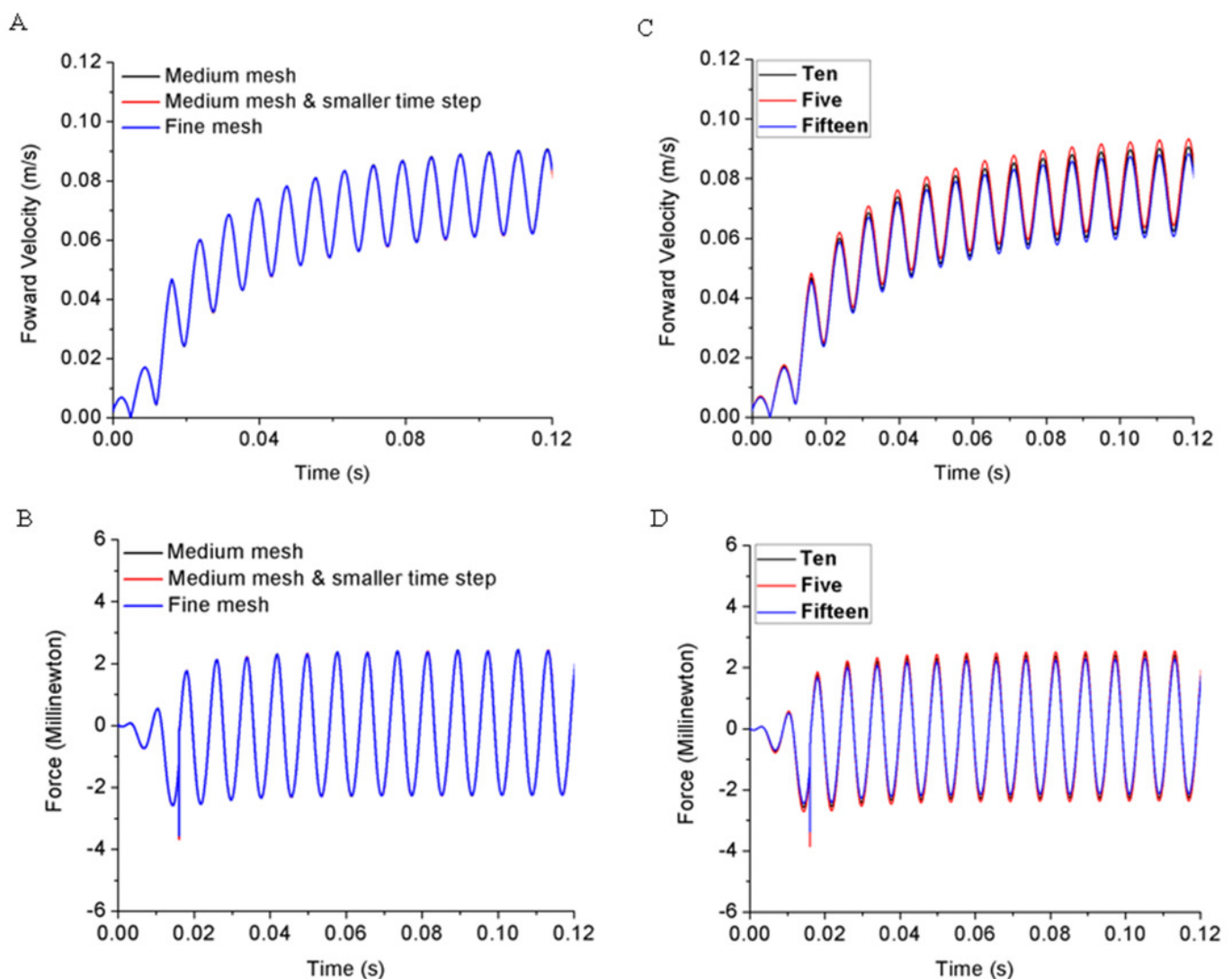
Figure 4

Jellyfish model

Jellyfish model. (A) Real jellyfish shape with dividing points. (B) Mathematical jellyfish model. theta1, theta2 and theta3 are intersection angles between each two segments. As the structure is symmetric to Y axis, values of intersection angles on the other side is equivalent but with reversed sign. Dmax represents maximum diameter of jellyfish model. (C) Local unstructured mesh around CFD jellyfish model
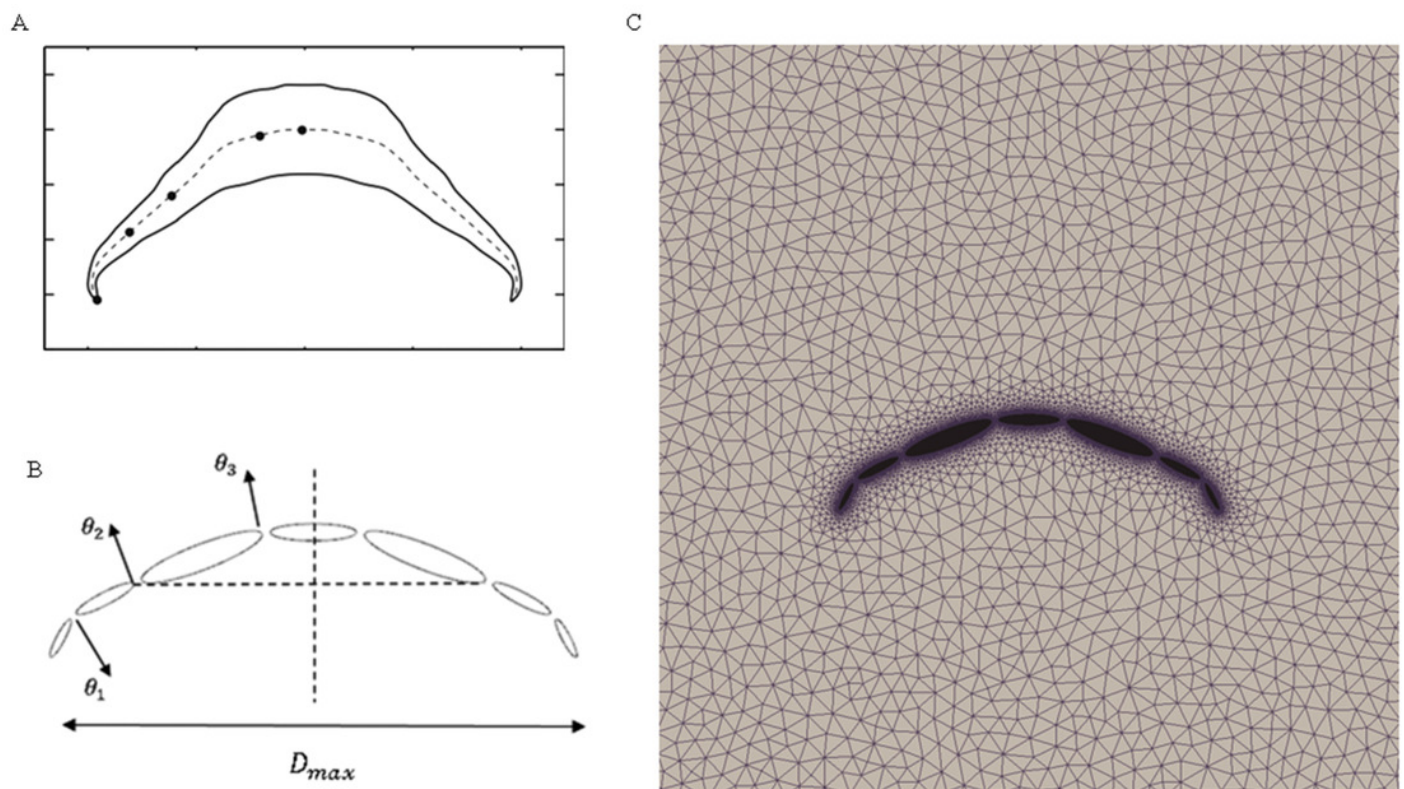
Figure 5

Validation results for periodic jellyfish movements

(A) Longitudinal centroid position for Re = 140. (B) Longitudinal centroid velocity for Re = 140. (C) Required input power for Re = 70. (D) Our CFD simulation result of vorticity at Re = 14 (E) Wilson & Eldredge's (2011) result of vorticity at Re = 14.
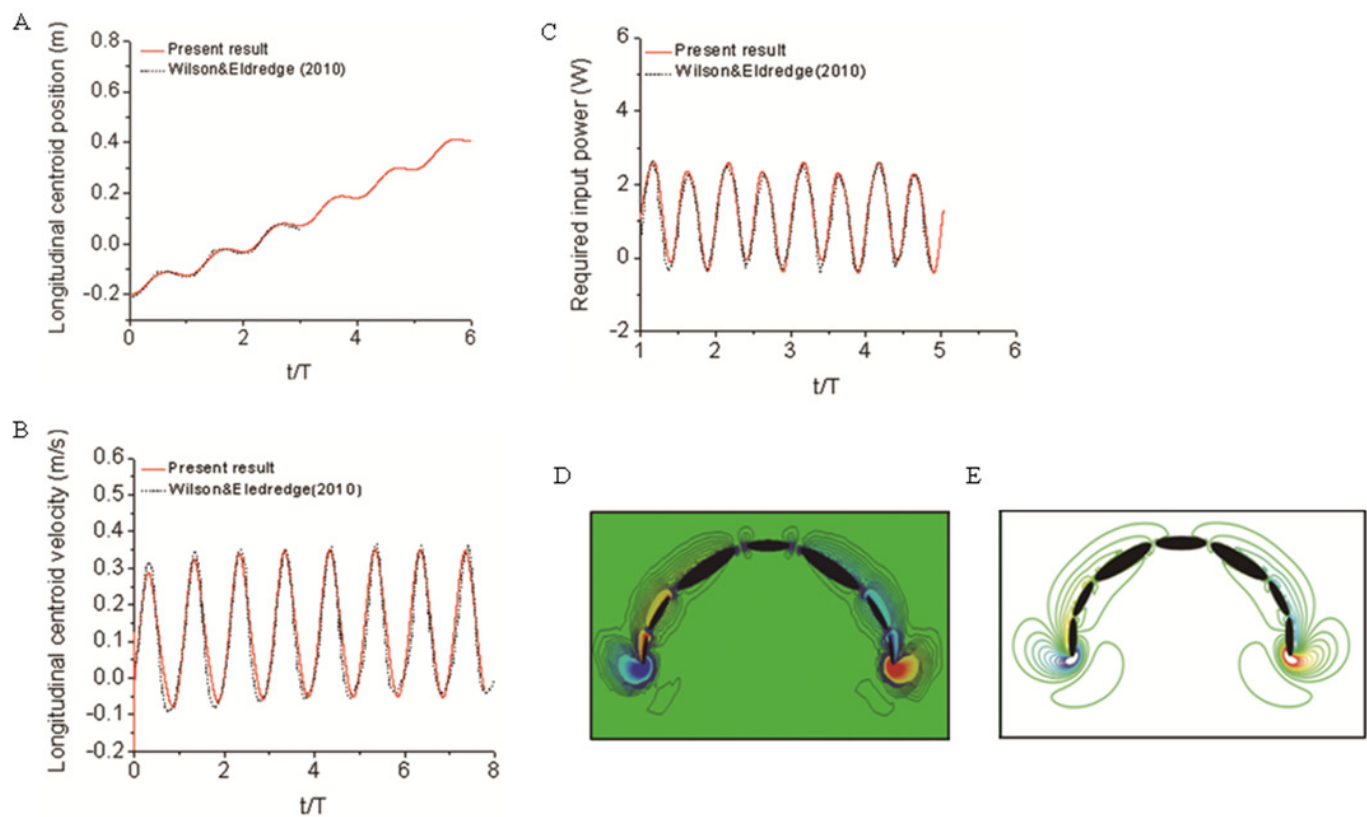
Figure 6

Comparison of simulated zebrafish data in global frame with experimentally observed zebrafish swimming

(A) Head angle (B) Tail angle (C) Forward swimming speed (D) Forward swimming speed for ten fish
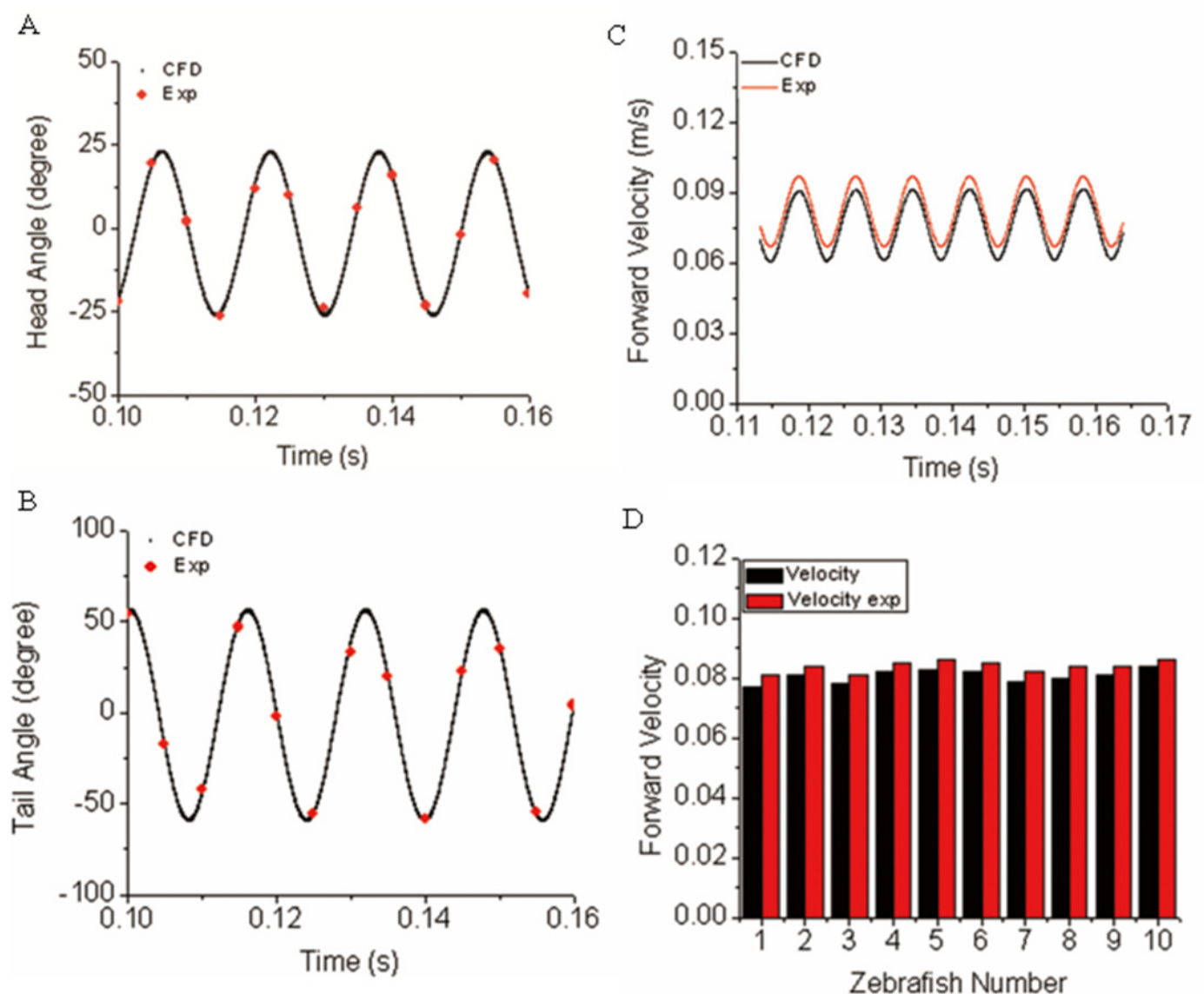
Figure 7

Vortex rings behind zebrafish larva for Q=0.5 at different time step within one period of time and the corresponding video record for the experiment

X-Y plane vorticity is a 2-D view of the 3-D vortices which can compare the body curvature with experiment results easier. From A-D, E-H and I-L, time steps are 0, T/3, 2T/3 and T for each column. T represents one period of time.
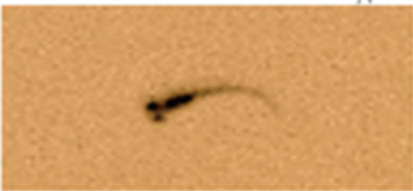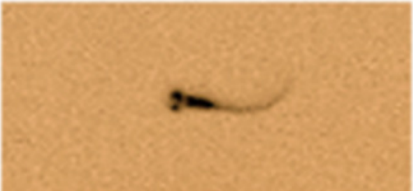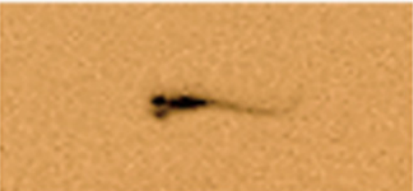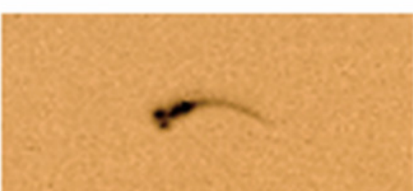
X-Y plane vorticity	Experiment	Q
A	E	I
B	F	J
C	G	K
D	H	L

Figure 8

Power distribution at three typical points and along fish body

(A) Real zebrafish picture (B) Hydrodynamic power for ten sample 5 dpf zebrafish larvae (C) Hydrodynamic force at three points (D) Velocity at three points (E) Averaged Hydrodynamic power for twenty fish larvae distribution of each body section along fish body (F) Averaged Mechanical power distribution of each joint along fish body for twenty fish larvae

A

B

C

D

E

F
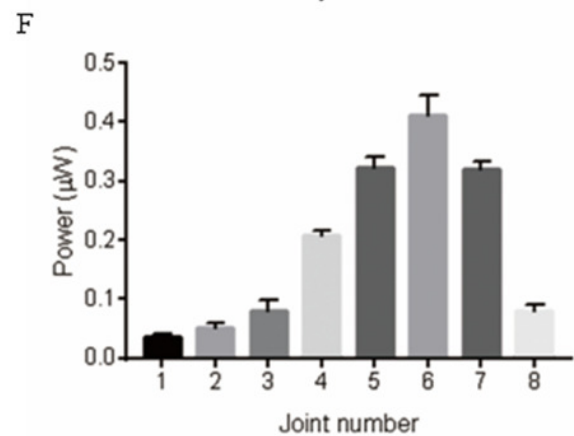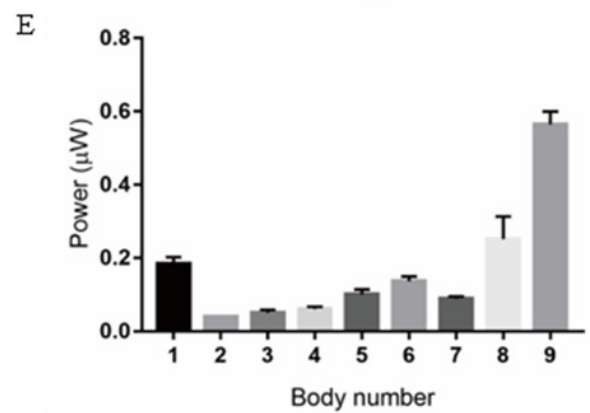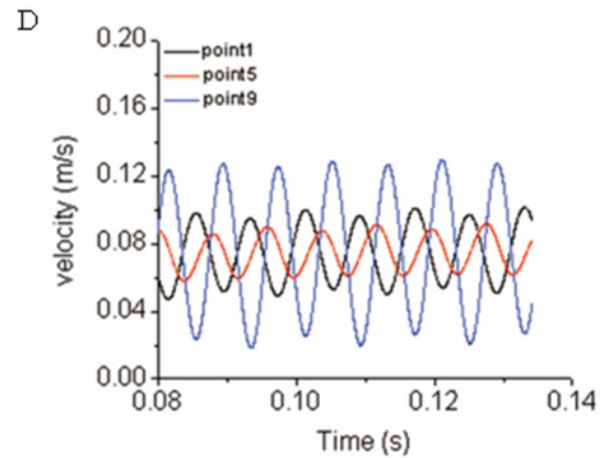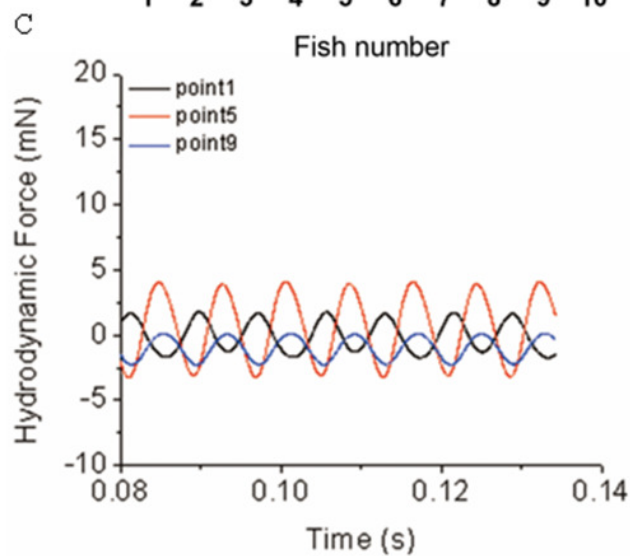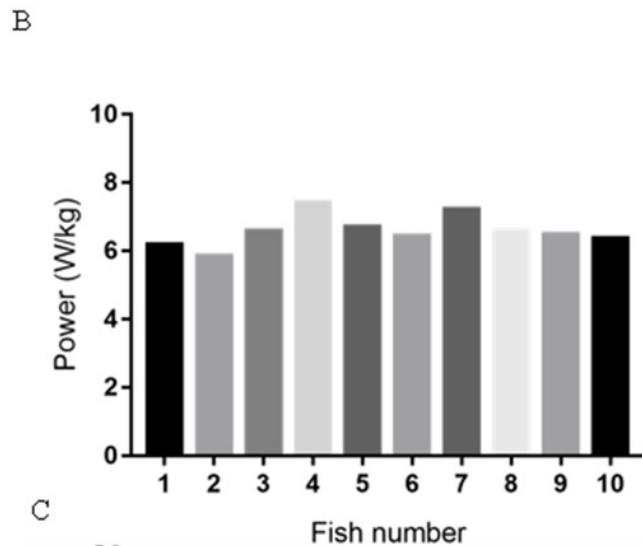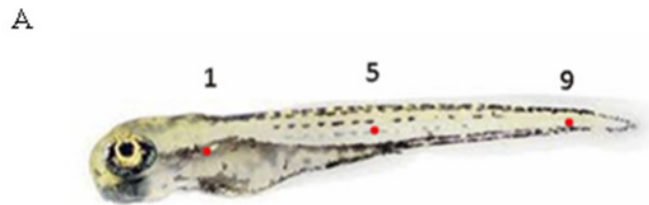
Figure 9

Comparisons between control group, 0.01% acetic acid treated group, 500 uM DPH treated group, and 100mg/L yohimbine treated group.

(A) Head angle (B) Forward velocity (C)Hydrodynamic power (D) Tail angle (E) Forward velocity comparison for control group and drug treated groups with two-tailed t-test for twenty fish in all, shown in mean (SD); P <0.0001: **** (F) Total hydrodynamic power generated by surrounding water with two-tailed t-test for control group and drug treated groups, shown in mean (SD); P < 0.0001: ****.

A

B

C

D

E

F
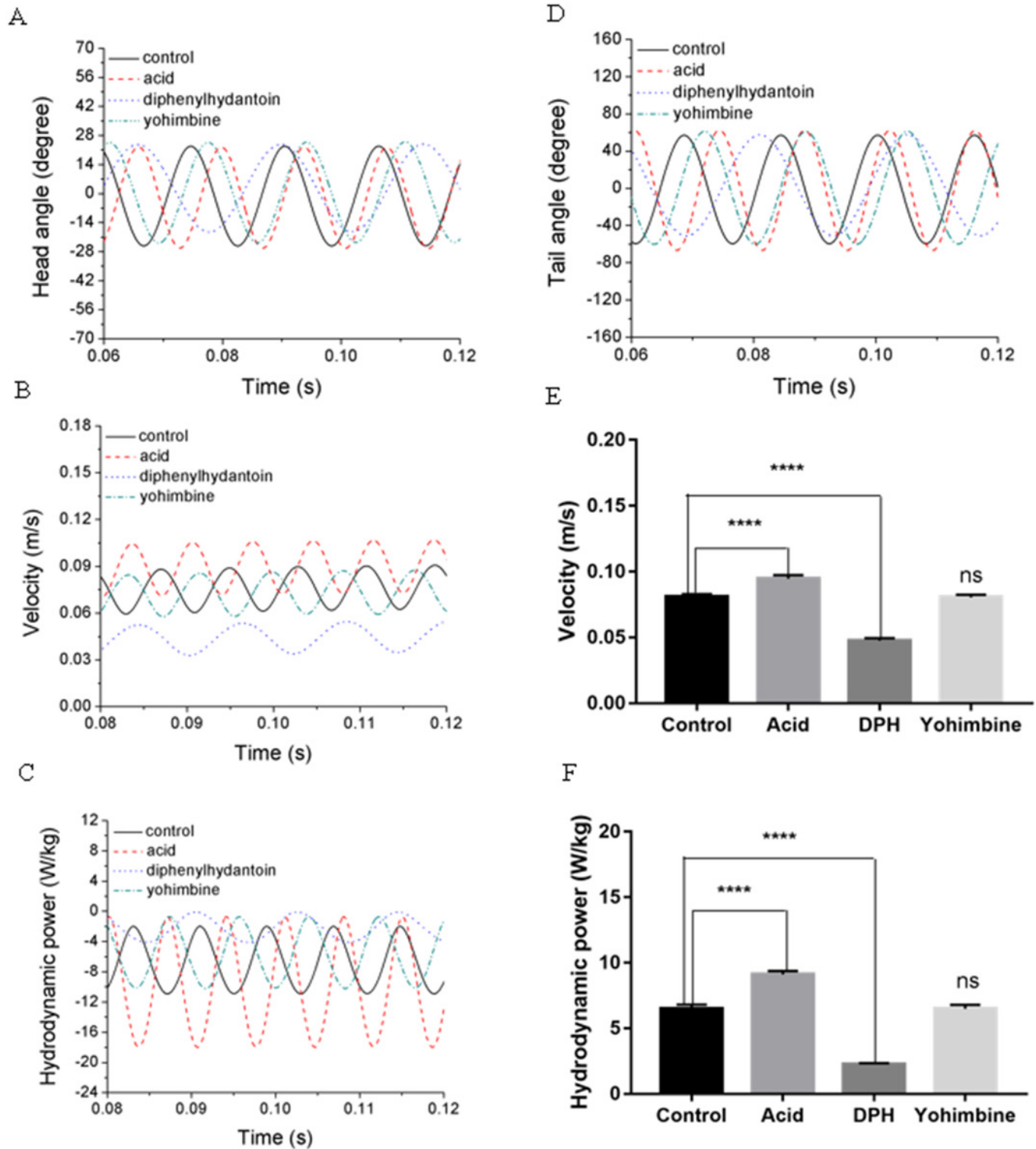
Figure 10

Vorticity comparisons in x-y plane between control group zebrafish and zebrafish exposed to drug treated groups within one period of time

For A-D, E-H, I-L and M-P, time steps are 0, T/3, 2T/3 and T for each column. T represents one period of time.
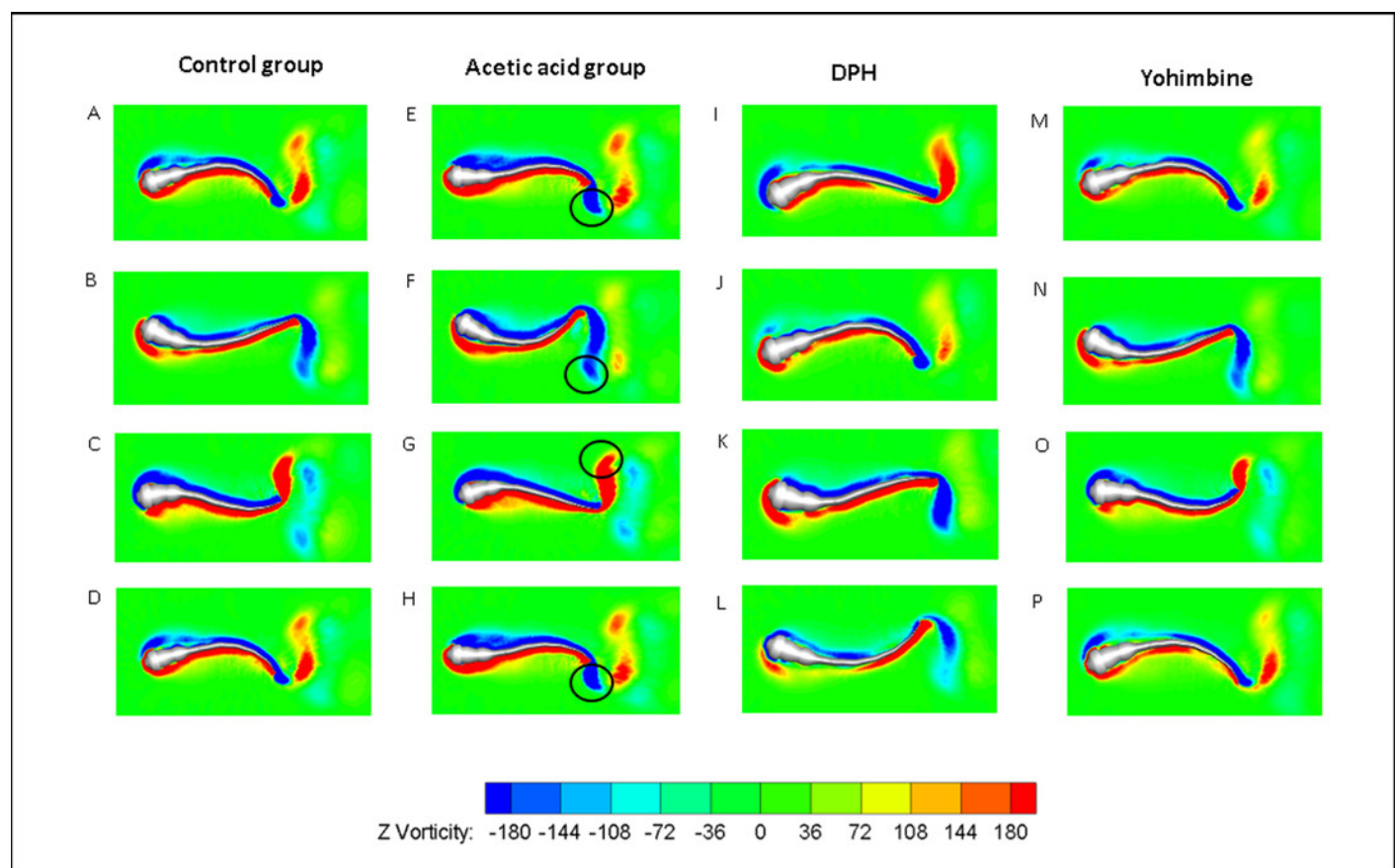
Detailed zebrafish larva body information

Body section number	Mass (mg)	Length (mm)
1	0.0385	0.4
2	0.0553	0.4
3	0.0425	0.48
4	0.0308	0.48
5	0.0212	0.48
6	0.019	0.48
7	0.011	0.48
8	0.009	0.48
9	0.003	0.32
Total	0.23	4

Detailed mechanical and hydrodynamic power values for 10 normal zebrafish larva numbered from fish1 to fish 10. S1-S9 represents the nine body sections. Hyd represents hydrodynamic power Mec represents mechanical power units of both are *uW*

		S1	S2	S3	S4	S5	S6	S7	S8	S9	cost of transport μJ/m
fish1	Hyd	0.16	0.04	0.05	0.06	0.09	0.14	0.08	0.26	0.55	79.97
	Mec	0.00	0.03	0.04	0.06	0.21	0.32	0.38	0.31	0.07	
fish2	Hyd	0.17	0.04	0.03	0.05	0.08	0.12	0.08	0.26	0.51	78.78
	Mec	0.00	0.03	0.04	0.06	0.20	0.31	0.36	0.30	0.07	
fish3	Hyd	0.19	0.04	0.06	0.07	0.11	0.14	0.09	0.26	0.56	84.33
	Mec	0.00	0.03	0.05	0.09	0.21	0.32	0.41	0.33	0.08	
fish4	Hyd	0.23	0.04	0.05	0.06	0.12	0.15	0.10	0.08	0.63	90.57
	Mec	0.00	0.04	0.06	0.12	0.22	0.37	0.49	0.34	0.08	
fish5	Hyd	0.18	0.04	0.05	0.07	0.12	0.16	0.09	0.28	0.55	80.64
	Mec	0.00	0.04	0.06	0.09	0.21	0.31	0.42	0.33	0.08	
fish6	Hyd	0.19	0.04	0.05	0.06	0.08	0.14	0.09	0.28	0.54	77.61
	Mec	0.00	0.03	0.05	0.06	0.20	0.33	0.40	0.31	0.08	
fish7	Hyd	0.18	0.04	0.06	0.06	0.10	0.14	0.09	0.28	0.59	85.56
	Mec	0.00	0.04	0.06	0.09	0.22	0.31	0.42	0.33	0.10	
fish8	Hyd	0.18	0.04	0.05	0.06	0.10	0.13	0.09	0.27	0.55	79.66
	Mec	0.00	0.04	0.04	0.07	0.20	0.32	0.41	0.31	0.08	
fish9	Hyd	0.18	0.04	0.05	0.06	0.10	0.13	0.09	0.27	0.55	79.18
	Mec	0.00	0.03	0.05	0.06	0.21	0.32	0.42	0.30	0.08	
fish10	Hyd	0.18	0.04	0.05	0.06	0.10	0.12	0.09	0.28	0.61	81.01
	Mec	0.00	0.04	0.06	0.09	0.21	0.31	0.41	0.33	0.09	